

# Effect of Different Perforations Shapes on the Thermal-hydraulic Performance of Perforated Pinned Heat Sinks

Amer Al-Damook<sup>1,2</sup>, J.L. Summers<sup>1</sup>, N. Kapur<sup>1</sup>, H. Thompson<sup>1</sup>

[mnajs@leeds.ac.uk](mailto:mnajs@leeds.ac.uk), [j.l.summers@leeds.ac.uk](mailto:j.l.summers@leeds.ac.uk), [n.kapur@leeds.ac.uk](mailto:n.kapur@leeds.ac.uk), [h.m.thompson@leeds.ac.uk](mailto:h.m.thompson@leeds.ac.uk)

<sup>1</sup>School of Mechanical Engineering, University of Leeds, UK

<sup>2</sup>Mechanical Engineering Department, University of Anbar, MOHESR, HCED, Iraq

**Abstract—** The benefits of using pinned heat sinks (PHSs) with multiple circular, square and elliptic perforations for electronic cooling applications are investigated using Computational Fluid Dynamics (CFD). A conjugate heat transfer analysis, using the RANS-based modified  $k-\omega$  turbulence model, is used to determine the effect of perforation shape on the cooling and hydraulic performance of PHSs. The numerical solutions indicate that the optimum design will be a compromise between elliptical perforations, which minimize pressure drop and mechanical fan power consumption, and circular perforations, which provide the most effective heat transfer. Employing staggered arrangements of perforated pins in PHS is also shown to be highly beneficial and to enable the power consumption required to cool a heat sink to a target temperature to be reduced significantly.

**Keywords—** Perforated pinned heat sinks, Conjugate heat transfer, Electronic component cooling.

## I. INTRODUCTION

Heat sinks with extended surfaces, such as plate fins or pins, are widely used in industry to improve heat transfer in critical cooling applications, for example the aerospace, automotive and nuclear industries, Sahin & Demir [1]-[2]. This requires their designers to achieve the required heat transfer levels subject to multiple constraints on their volume, mass, cost etc. The main motivation of the present study is the use of PHSs in the air cooling of electronics, which remains the most common method of reducing the temperature of CPUs below critical values in order to provide acceptable component reliability [3].

A number of recent studies have explored the performance benefits of perforating plate fins in plate fin heat sinks (PFHSs) or perforating the pins in pinned heat sinks (PHSs). These have shown that perforations can increase simultaneously heat transfer and reduce the mechanical fan power needed to overcome the pressure losses [3]-[4]. The plate fins in PFHSs can be perforated either longitudinally, along the fins, or laterally across them. Shaeri et al [5]-[8] considered the effect of longitudinal perforations for both laminar and turbulent flows and demonstrated that these can enhance heat transfer while reducing pressure drop by reducing the size of the recirculation

zones (wakes) behind the plate fins. Ismael et al [9]-[11] extended this work to consider the effect of the longitudinal perforation shape (circular, square, triangular and hexagonal) on performance and found that both circular and hexagonal perforations provide significant enhancements.

Lateral plate fin perforations in PFHSs have also been considered. Yaghoubi et al [12]-[13] showed that lateral perforations are ineffective for laminar airflows but that they do lead to enhanced heat transfer for turbulent flows. Ismail et al [14] later considered the effect of lateral perforation shape (circular, square, triangular and hexagonal) for turbulent airflows. They found that hexagonal perforations yielded the highest heat transfer rate while triangular ones minimize the friction coefficient.

In comparison with PFHSs, relatively few studies have considered the effect of pin perforations on the performance of PHSs. Sahin and Demir [15]-[16], for example, studied the effect of single circular or square perforations for PHSs with in-line pin arrays, while Amol and Farkade [17] considered the effect of staggered arrangements of pins with single perforations of circular cross section. These and other studies have found consistently that a single perforation leads to an enhancement in heat transfer and a reduction in pressure drop compared to equivalent solid pin systems. In addition to the increased area for heat transfer, these enhancement are due to localized jet flows through the perforations which increase local heat transfer by shear-induced mixing and reduce pressure drop by alleviating the recirculation zones that form behind solid pins.

Al-Damook et al [3] used complementary experimental and numerical methods to investigate the effect of multiple (up to five) pin perforations in the performance of PHSs. They demonstrated that multiple pin perforations can provide significantly greater heat transfer and pressure drop benefits than for single perforations, and that these benefits increase monotonically as the number of perforations increases, while the location of the perforations has only a relatively minor influence on performance. With five perforations, they demonstrated an 11% increase in heat transfer and a 16% reduction in pressure drop compared to an equivalent solid pin PHS. The benefits of using perforations on strip fins where the cross-sectional aspect ratio of the fins are between those for plate fins (high aspect ratio) and pins fins (aspect ratio  $\approx 1$ ) have been investigated recently by Al-Sallami

et al [18]. They found that perforating the strip fins provides substantial enhancements in heat transfer, with reduced pressure loss and heat sink mass.

In This paper presents the first detailed investigation into the influence of the shape of pin perforations on the thermal and hydraulic performance of PHSs. It extends the recent studies of Ismail et al [9]-[11] and Al-Damook et al [3] to compare the effect of pin perforation shape (circular, square and elliptical) for pins with the three perforations shown in Fig. 2. The paper is organized as follows. In section 2 the numerical conjugate heat transfer model is described while section 3 describes the validation of the numerical method and the results of the numerical investigation. Conclusions are drawn in section 4.

## II. NUMERICAL METHOD

### A. Physical Model

Thermal airflows over PHSs with a base of 50mm length ( $L$ ) $\times$ 50mm width ( $W$ ) $\times$ 2mm thickness ( $t$ ) and 64 pin fins of height 10mm and diameter 2mm in an in-line array are considered, Fig. 1. Airflows past PHSs with the pins perforated with three circular, square or elliptical perforations aligned in the direction of the airflow, as shown in Fig. 2, are solved numerically and compared with the benchmark case with solid pins. The inlet air temperature is set to 25°C while the inlet air velocity is varied from 6.5m/s to 12m/s, leading to Reynolds numbers in the range 3500-6580 based on a length scale given by the hydraulic diameter of the duct  $Dh=2H.W/(H+W)$ , where  $H$  and  $W$  are the height and width of duct in which the heat sink is located, respectively. The PHS is aluminium, with thermal conductivity  $k=202$  W/m.K.

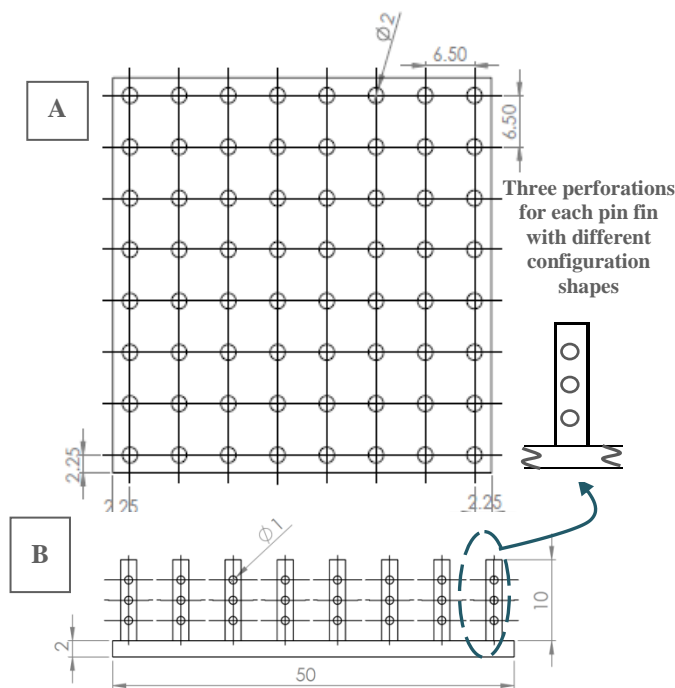


Fig. 1: (A) Plan view and (B) side view of the pin fins heat sink being analysed

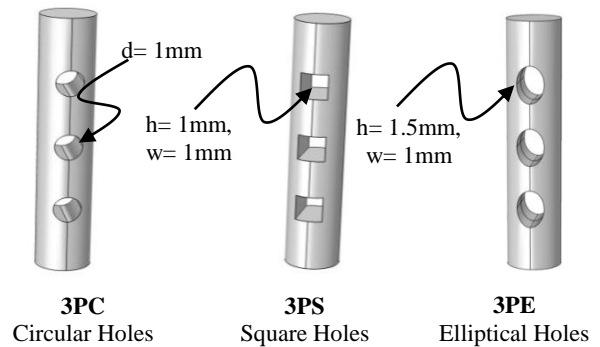


Fig. 2: Three perforations shapes for each pin fin designs considered, with same numbers and locations of perforations and all dimensions in mm.

### B. Conjugate Heat Transfer Model

In the conjugate heat transfer model the rate of heat conduction through the aluminium heat sink is balanced by the convective heat transfer into the moving air stream, through a coupled boundary condition at the solid/fluid interface of the heat sink [14], as illustrated in Fig. 3. The energy equations in the fluid and solid domains are given by:

For the fluid domain

$$\underline{U} \cdot \rho \cdot c_p \nabla T_f = \nabla \cdot \left[ \left( k_f + \frac{c_p \cdot \mu_T}{Pr_T} \right) \nabla T_f \right] \quad (1)$$

For the solid domain

$$\nabla \cdot (k_s \cdot \nabla T_s) = 0 \quad (2)$$

where  $\underline{U}$  is fluid (air) velocity;  $T_f$  and  $T_s$  are fluid and solid temperature, respectively;  $\mu_T$ ,  $Pr_T$ ,  $k_f$  and  $k_s$  are the turbulent viscosity, the turbulent Prandtl number, the thermal conductivity of the fluid and solid, respectively.

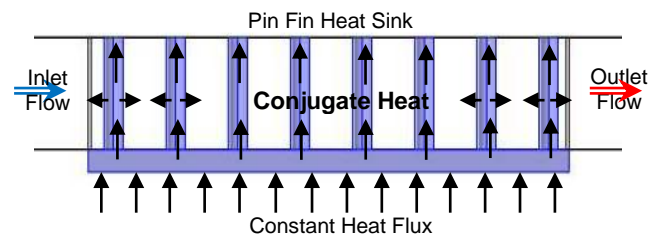


Figure 3: Conjugate heat transfer model of pin fin heat sink [3]

### C. Airflow Model

Airflow over the PHSs is assumed incompressible, steady state, and turbulent. Several previous studies have used the Reynolds-Averaged Navier-Stokes (RANS) equations to model turbulent airflow through heat sinks successfully, see for example [19]-[20]. Time-averaging the continuity, momentum and energy equations with variables decomposed into mean and fluctuating components leads to the Reynolds-Averaged Navier-Stokes (RANS) equations, namely:

$$\nabla \cdot \underline{U} = 0 \quad (3)$$

$$\frac{\partial \underline{U}}{\partial t} + \nabla \cdot (\underline{U} \underline{U}) = \frac{1}{\rho} \nabla \cdot (\underline{\sigma} - \rho \overline{U' U'}) \quad (4)$$

where  $\underline{\sigma} = -p \underline{I} + \mu (\nabla \underline{U} + [\nabla \underline{U}]^T)$  and  $-\rho \overline{U' U'} = \mu_t (\nabla \underline{U} + [\nabla \underline{U}]^T) - 2/3 (\rho k \underline{I})$  are the Newtonian and Reynolds Stress tensors respectively,  $\mu$  is the air viscosity,  $\rho$  its density,  $\underline{U}$  and  $\overline{U'}$  the average and turbulent fluctuation velocity vectors respectively,  $p$  is the pressure and  $\underline{I}$  the unit tensor.

The incompressible RANS equations are solved with the energy equation for the temperature field in the fluid,  $T_f$ , with a heat source  $\dot{Q}$  Watts, using the following equation

$$\frac{\partial T_f}{\partial t} + \underline{U} \cdot \nabla T_f = \left( \frac{\nu}{Pr} + \frac{\nu_t}{Pr_t} \right) \nabla^2 T_f + \frac{\dot{Q}}{\rho C_p} \quad (5)$$

where  $C_p$  is the specific heat capacity of the air,  $Pr$  and  $\nu$  are the Prandtl number and kinematic viscosity of the air respectively and the subscript  $t$  indicates their turbulent counterparts.

Following Zhou & Catton [19] and Leung & Probert [20], the thermal airflow through the heat sink is modelled using the  $k$ - $\omega$  SST model with automatic wall function treatment. As discussed above and following Al-Damook et al [3], who found that with maximum temperature differences of  $62^\circ\text{C}$  for polished aluminium fins, the radiative heat loss is only 1% of the total heat transfer rate, radiative heat transfer is neglected. Air density and viscosity are assumed to be constant and equal to those at the inlet temperature of  $25^\circ\text{C}$ . This model combines the accurate formulation of the  $k$ - $\omega$  model in the near-wall region with the free-stream independence of the  $k$ - $\epsilon$  one in the far field, and has been shown to predict highly separated flows accurately in a number of previous validation studies [19]-[21].

The equations for the SST model are:

$$\frac{\partial(\rho k)}{\partial t} + \nabla(\rho k \underline{U}) = \tilde{P}_k - \beta^* \rho k \omega + \nabla \cdot [(\mu + \sigma_k \mu_t) \nabla k] \quad (6)$$

$$\begin{aligned} \frac{\partial(\rho \omega)}{\partial t} + \nabla(\rho \omega \underline{U}) &= \alpha \rho S^2 - \beta \rho \omega^2 + \nabla \cdot [(\mu + \sigma_\omega \mu_t) \nabla \omega] \\ &+ 2(1 - F_1) \rho \sigma_{\omega_2} \frac{1}{\omega} \nabla k \cdot \nabla \omega \end{aligned} \quad (7)$$

where the blending function  $F_1$  is defined by

$$F_1 = \tanh \left\{ \min \left[ \max \left( \frac{\sqrt{k}}{\beta^* \omega y}, \frac{500 \nu}{y^2 \omega} \right), \frac{4 \rho \sigma_{\omega_2} k}{C D_{k\omega} y^2} \right] \right\}^4$$

in which

$$C D_{k\omega} = \max \left( 2 \rho \sigma_{\omega_2} \frac{1}{\omega} \nabla k \cdot \nabla \omega, 10^{-10} \right)$$

The turbulent eddy viscosity is computed from

$$\nu_t = \frac{a_1 k}{\max(a_1 \omega, S F_2)} \quad (8)$$

where  $S$  is the invariant measure of the strain rate and  $F_2$  is a second blending function defined by

$$F_2 = \tanh \left( \left[ \max \left\{ 2 \frac{\sqrt{k}}{\beta^* \omega y}, \frac{500 \nu}{y^2 \omega} \right\} \right]^2 \right)$$

To limit the growth of turbulence in stagnation regions, a production limiter is used in the SST model.

$$P_k = \mu_t \frac{\partial u_i}{\partial x_j} \left( \frac{\partial u_i}{\partial x_j} + \frac{\partial u_j}{\partial x_i} \right) \rightarrow \tilde{P}_k = \min(P_k, 10 \beta^* \rho k \omega)$$

The constants for this model are

$$\beta^* = 0.09, \alpha_1 = 0.555, \beta_1 = 0.075, \sigma_{k1} = 0.85, \sigma_{\omega_1} = 0.5, \alpha_2 = 0.44, \beta_2 = 0.0828, \sigma_{k2} = 1, \sigma_{\omega_2} = 0.856.$$

#### D. Solver Settings

The grid is composed of dense tetrahedral mesh elements to improve the quality of the numerical prediction near curved pin surfaces. A commercial finite volume method (FVM)-based code, ANSYS FLUENT [22] is used to solve the fully coupled momentum and energy equations, using second order upwinding, while continuity is satisfied using the SIMPLE method in which the velocity components are first calculated from the Navier–Stokes equations using a guessed pressure field. Computation is started first by solving the continuity, momentum,  $k$  and  $\omega$  equations to determine the flow field and then the energy equation to find the temperature field in the computational region. The procedure continues until the sum of the residuals of the continuity and momentum equations in each cell is less than  $10^{-4}$  and the residuals of the energy equations are smaller than  $10^{-6}$ .

#### E. Boundary Conditions

The computational problem is reduced in size by exploiting the symmetry of the PHS to apply symmetry boundary conditions along the sides of the channel (Fig. 4). This inlet and outlets of the domain should be far enough from the entrance and exit regions of the heat sinks to avoid boundary effects such as reverse flow at the exit. To avoid these problems, the entrance and exit regions are a distance of  $12.5d$  from the heat sink.

The fluid and thermal conditions are:

1- At the inlet:

$$6.5 \text{ m/s} \leq U \leq 12 \text{ m/s}, T_{ai} = 25^\circ\text{C}$$

2- At the PHS surfaces:

$$U = 0 \text{ m/s}, k_f \cdot \frac{dT_f}{dn} = k_s \cdot \frac{dT_s}{dn}$$

3- At the bottom base wall of the heat sink:

$$U = 0 \text{ m/s}, \dot{Q} = 20000 \text{ W/m}^2$$

4- At the outlet:  $P = P_{\text{gauge}} = 0 \text{ Pa}, \frac{dT}{dx} = 0$

5- At the other surfaces:

$$U=0\text{m/s}, \frac{dT}{dz} = 0$$

6- At the symmetry boundaries:

$$\frac{du}{dy} = 0, \frac{dT}{dy} = 0$$

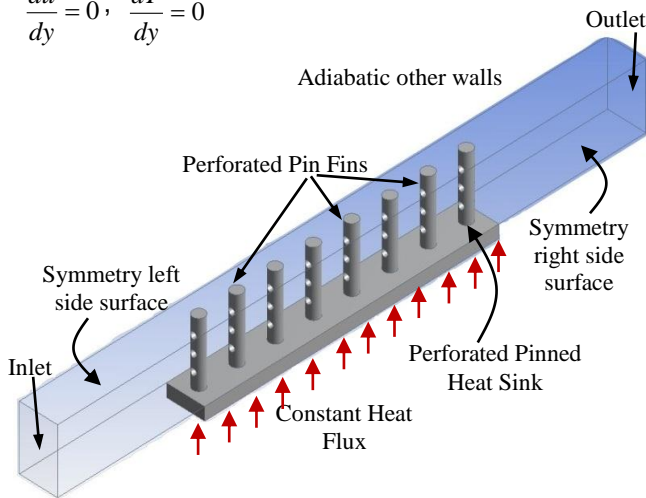


Fig. 4: Schematic diagram of the flow domain used in the CFD analyses, shown eight perforated pin fins

#### F. Post Processing

The CFD analysis is used to determine the velocity and temperature fields as well as the Nusselt number ( $Nu_T$ ), based on the total surface area, pressure drop ( $\Delta P$ ), fan power ( $P_{fan}$ ) and CPU temperature ( $T_{case}$ ), as follows [23].

The heat transfer rate is represented by Nusselt number:

$$Nu_T = h.L/k_{air} \quad (9)$$

where  $h$  is the heat transfer coefficient ( $W/K.m^2$ ),  $L$  the length of the heat sink in the flow direction (m) and  $k_{air}$  the thermal conductivity of the air ( $W/m.K$ ). Now

$$h_T = h_T = \dot{Q} A_T / (T_s - T_m) \quad (10)$$

where  $\dot{Q}$  is the power applied to the base (W),  $A_T$  is the total surface area including the pin and perforation surface areas ( $m^2$ ),  $T_s$  is the pin heat sink surface temperature and  $T_m$  is the average bulk mean temperature  $T_m = (T_{in} + T_{out})/2$ .

The fan power required to drive the fluid through the heat sink can be evaluated as [24]-[25],

$$P_{fan} = U.A_p.\Delta p \quad (11)$$

where  $U$ : inlet air velocity (m/s),  $A_p$  ( $m^2$ ): cross-sectional area of the flow passage of the heat sink =  $H.S.(N-1)$ .

### III. RESULTS AND DISCUSSION

#### A. Grid Independence

CFD solutions are obtained on a range of grids, where the number of cells varies between 98,000 and 210,000. The effect of grid resolution on  $Nu_T$ ,  $T_{case}$  and  $\Delta P$  is shown in Table 1, which demonstrates that

increasing the number of cells beyond 120,000 results in typically a 2% change in these parameters. All numerical results reported below have been obtained using 150,000 cells.

Table 1: Grid independence study data for different perforated pin fin heat sinks

| Square Perforated Pins (3SP) Cells   | $Nu_T$ | $T_{case}$ ( $^{\circ}C$ ) | $\Delta P$ (Pa) |
|--------------------------------------|--------|----------------------------|-----------------|
| 115771                               | 385.4  | 63.8                       | 89.6            |
| 129567                               | 390.6  | 62.5                       | 89.9            |
| 150792                               | 394.0  | 62.0                       | 90.3            |
| 166555                               | 397.0  | 62.3                       | 90.6            |
| Circular Perforated Pins (3CP) Cells | $Nu_T$ | $T_{case}$ ( $^{\circ}C$ ) | $\Delta P$ (Pa) |
| 113000                               | 373.6  | 63.0                       | 92.7            |
| 123689                               | 379.7  | 62.3                       | 94              |
| 161916                               | 395.2  | 61.3                       | 93.6            |
| 202678                               | 400.0  | 61.7                       | 95.2            |
| Elliptic Perforated Pins (3EP) Cells | $Nu_T$ | $T_{case}$ ( $^{\circ}C$ ) | $\Delta P$ (Pa) |
| 98125                                | 354.2  | 64.5                       | 87.9            |
| 127976                               | 374.0  | 62.9                       | 86.7            |
| 172354                               | 384.8  | 62.3                       | 86.9            |
| 209001                               | 389.6  | 61.4                       | 86.1            |

#### B. Validation against Previous Studies

It is important that any numerical model should be carefully validated before it is used for design purposes. The experimental data of Yang et al [26] provides a useful validation case for predictions of the heat transfer coefficient ( $h_T$ ) and the pressure drop ( $\Delta P$ ) over solid PHSs. Fig. 5 indicates that the % error between predicted the experimental and numerical results is less than 2%, and 5%, respectively. It is clear that the heat transfer coefficient and the pressure drop measurement from the previous experimental study are in good agreement with those present predicted CFD. Other validations of the numerical approach used here can be found in Al-Damook et al [3]-[4]. The numerical model is now used to explore the effect of employing the perforated pins shown in Fig. 2 on the thermal and hydraulic performance of PHSs.

#### C. Effect of Perforation Shape on Pressure Drop and Mechanical Power Consumption

Fig. 6 explores the effect of perforations shape and inlet air velocity  $6.5\text{m/s} \leq U \leq 12\text{m/s}$  on the pressure drop,  $\Delta P$ , over a PHS with the 8x8 array of pins shown in Fig. 1. The elliptically-perforated pins (3EP) have the lowest pressure drops, which are typically around 12% lower than for the solid pins (0P). The fan power required to drive the air through the heat sink, ignoring losses due to fan inefficiency, is defined by

$P_{fan}=UA \Delta P$ , where  $U$  is the inlet air velocity and  $A$  is the cross-sectional area of the flow passage of the heat sink. Fig. 7 shows the corresponding data for the effect on fan power,  $P_{fan}$ : power consumption for the square, circular and elliptical perforations is approximately 7%, 9%, and 12% lower than for solid pins. The reductions in pressure drop and power consumption increase with the perforation volume and hence the porosity of pins increases, providing less resistance to air flow through them.

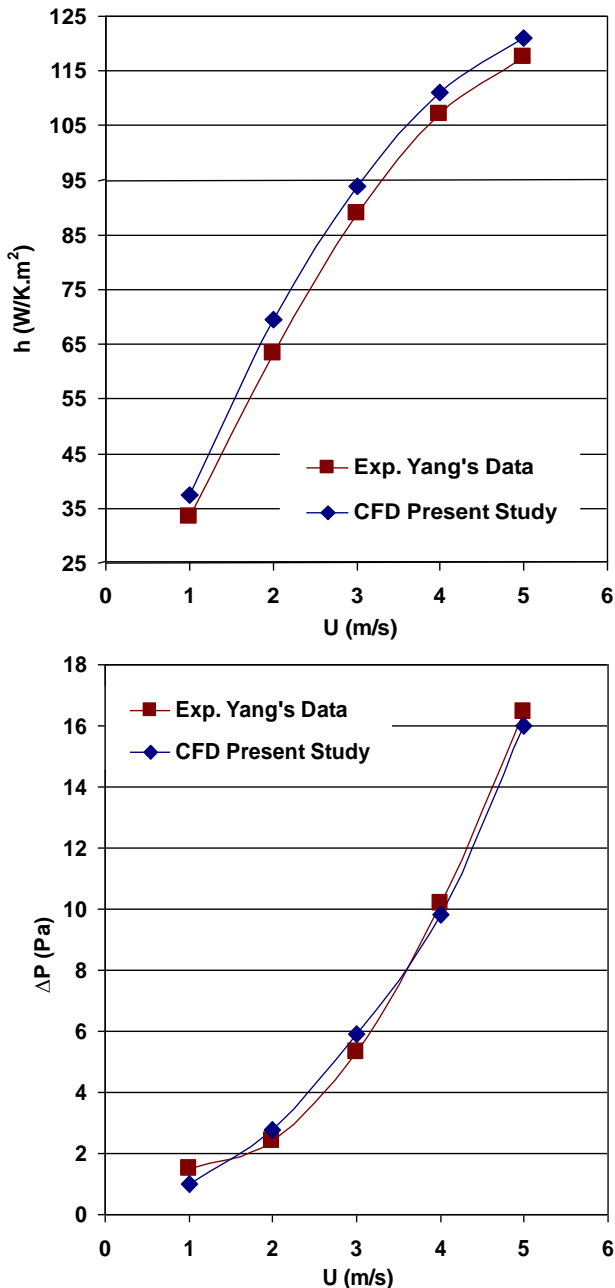


Fig. 5: Comparison between CFD predictions and the experimental data of Yang et al [26] of heat transfer coefficient and pressure drop.

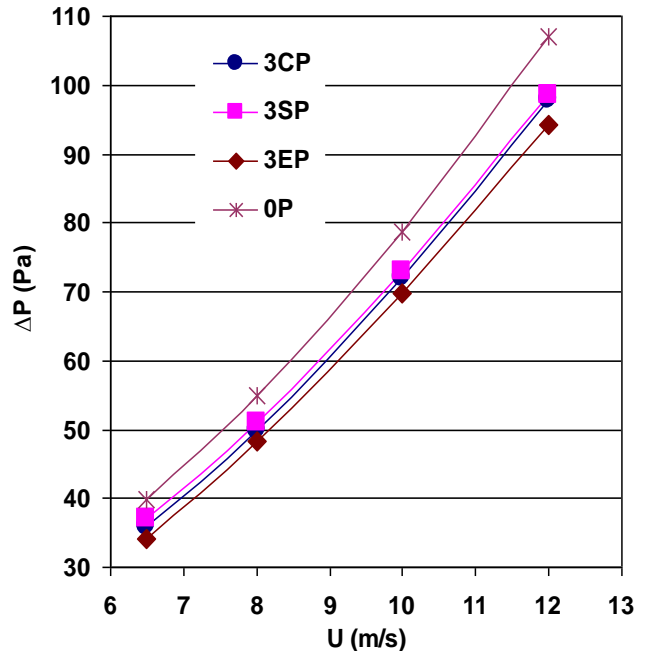


Fig. 6: Effect of perforation shapes on the pressure drop with various inlet air velocities

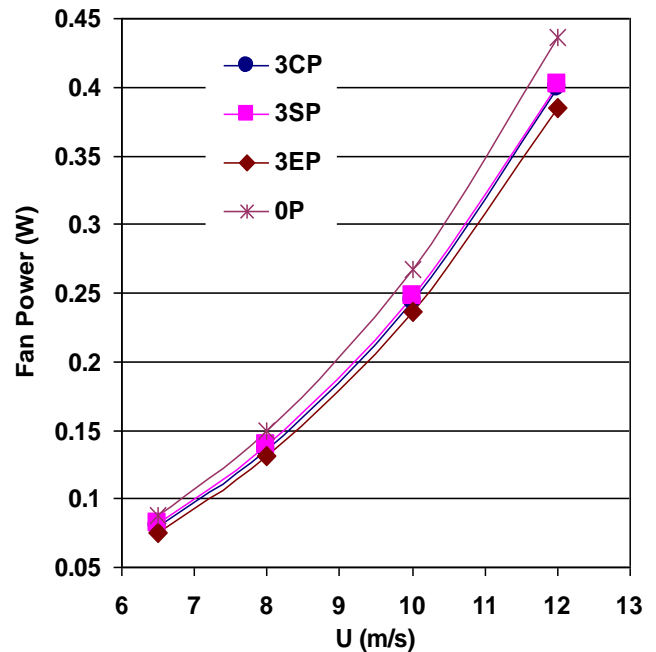


Fig. 7: Effect of perforation shapes on the fan power of pinned heat sinks

#### D. Effect of Perforation Shape on Heat Transfer

Fig. 8 shows the effect of the perforation shape on the Nusselt number,  $Nu_T$ , for Reynolds numbers in the range  $3500 \leq Re \leq 6580$ . The data show that the perforations increase  $Nu_T$  in all cases, and that the largest enhancement compared to the solid pin cases (0P) is for circular perforations (~9%) while the square and elliptical perforations lead to typical enhancements of between 4%. Fig. 9 shows the mean air velocity through each pin in the heat sink for the three perforated pin cases with  $U=12\text{m/s}$ . The finding that the circular perforations have the largest velocities is consistent with previous studies which have suggested

that the increased heat transfer with perforations is due to the formation of air jets flowing through the perforations which enhance convective heat transfer around them, see Sara et al. [27].

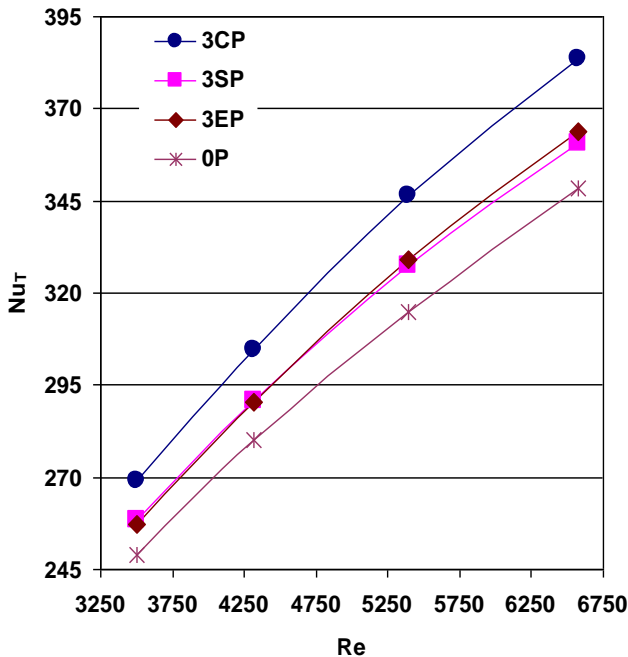


Fig. 8: Nusselt number for solid and different perforation shapes with various  $Re$

perforated pins at an inlet airflow at 10m/s ( $Re= 5393$ ). For the solid pins, the base plate temperatures vary between approximately 58.5°C and 71°C, whereas pins with circular, square and elliptical perforations temperatures range between 52°C to 66.5°C, 52.5°C to 67°C and 53°C to 67°C, respectively.

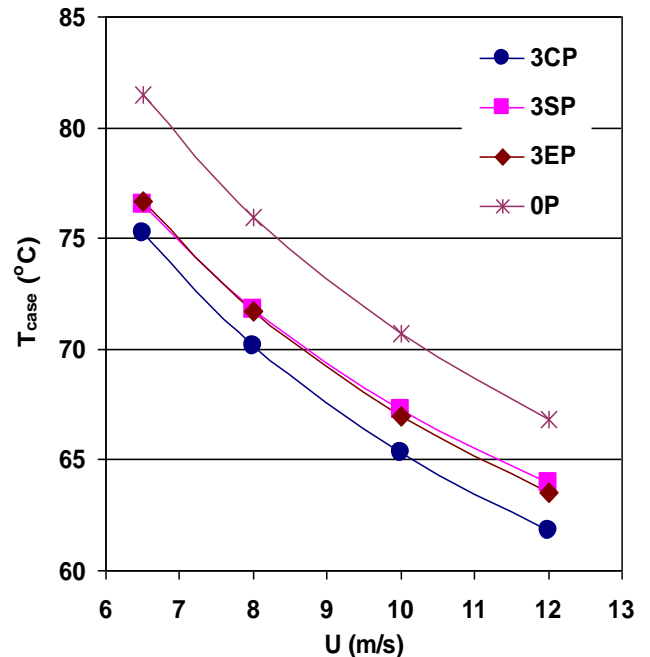


Fig. 10: Heat sink base temperature with perforation shapes and inlet air velocity

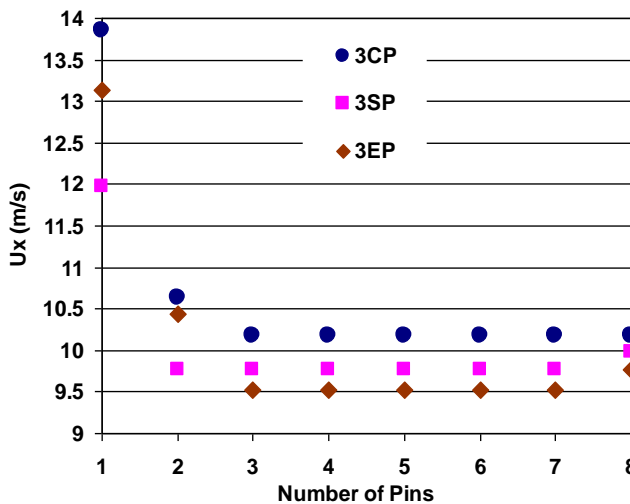


Fig. 9: Variation of mean local air velocity through the different pin perforations shapes

In electronics cooling the principal role of the heat sink is to remove heat in order to restrict the temperature of the CPU below critical temperatures to ensure performance reliability. Fig. 10 shows the effect of perforation shape on the average heat sink base plate temperature,  $T_{case}$ , for inlet air velocities  $6.5\text{m/s} \leq U \leq 12\text{m/s}$ . The improved heat transfer with the circular perforations results in values of  $T_{case}$  that are typically 8% smaller than for a PHS with solid pins, whereas those for the square and elliptical perforations are roughly 6% smaller than with solid pins. Fig. 11 compares the surface temperature distribution of a PHS with solid pins (0P) and those obtained with the

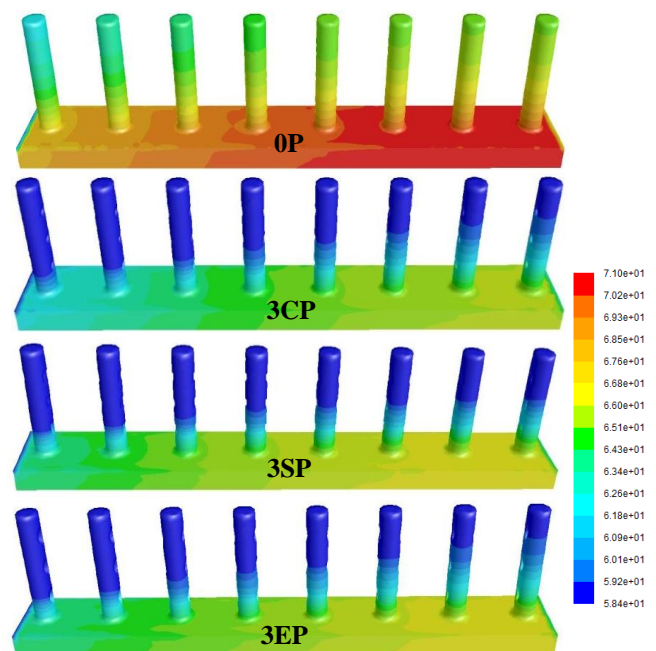


Fig. 11: Temperature distribution through perforated pinned heat sinks: 0P, 3CP, 3SP and 3EP models at  $Re=5393$

#### E. Effect of Pin Arrangement

The effects of employing the staggered arrangement of pins fins, shown in Fig. 12, are now investigated. Fig. 13 compares the pressure drop,  $\Delta P$ , across a PHS for both an in-line and a staggered array of solid (0P) and perforated (3CP) pins. The pressure

drop across the staggered array is approximately 30% greater than the corresponding in-line array for both the solid and perforated pins. The main reason for this is that the staggered arrangement increases the flow blockage in the airflow direction.

Fig. 14 shows the effect of a staggered pin arrangement for both solid and perforated pins (3CP) on the resultant CPU temperature as a function of fan power consumption. It shows that the staggered arrangement enables as lower CPU temperature to be achieved for a given mechanical power consumption. At the higher power consumptions, the CPU temperature of the staggered array of perforated pins is approximately 5°C lower than for the in-line arrangement while those of the solid pins are approximately 4°C lower. The improved heat transfer with the staggered arrangement of pins is due to increased turbulent mixing and convection from the PHS, Yang et al [26]. The performance of the in-line and staggered arrays of pins are compared in Table 3.

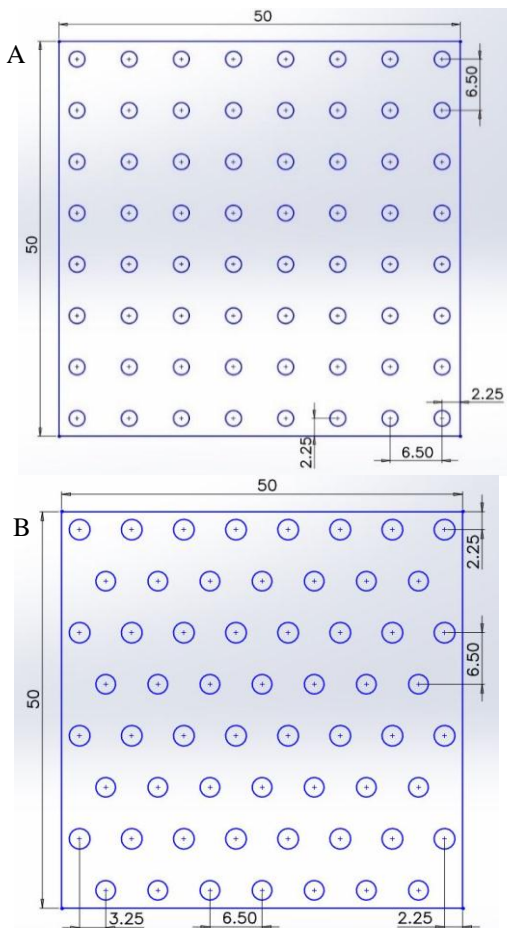


Fig. 12: Schematic diagram of pinned heat sink with (A) in-line and (B) staggered [18] arrays

#### F. Effect of Perforations on Heat Sink Weight

Minimizing the weight of consumer electronics is a key design goal and a number of studies have attempted to either maximize the heat transfer rate for a given fin weight or minimize the weight for a specified heat transfer rate [11]. Perforations reduce the mass of the pins and for the circular, square and

elliptical perforated pin fins these lead to reductions in mass of the pins of 15%, 19% and 22% respectively. The total weight of the PHS,  $W_T$ , is given by the expressions

$$V_T = V_{Base} + V_{Pins} \quad (12)$$

$$W_T = \rho_{Al} \times V_T \quad (13)$$

where  $V_{Base}$  is the volume of the base of the PHS,  $V_{Pins}$  the total volume of its pins,  $V_T$  the total volume of the PHS and  $W_T$  its total weight, where the density of aluminium  $\rho_{Al} = 2700 \text{ Kg/m}^3$ . Thus, the total weight reduction is approximately 4% for circular perforated pins (3CP) and 5% for both square perforated pin fins (3SP) and elliptic perforated pin fins (3EP).

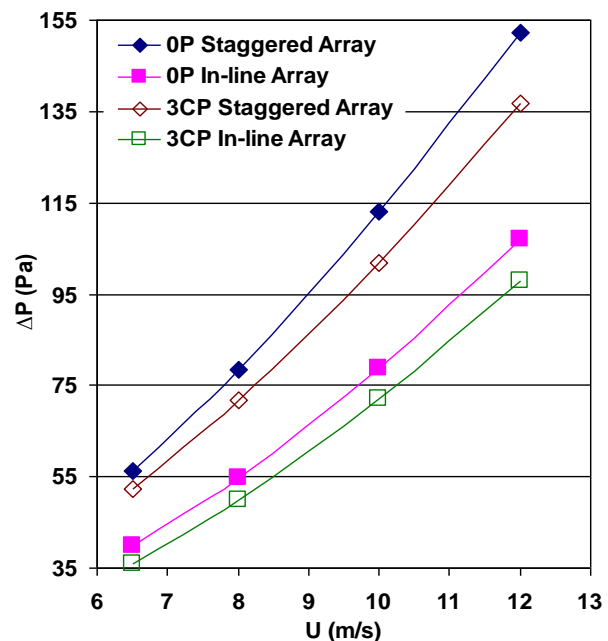


Fig. 13: Effect pins array on pressure drop with variation Reynolds number for solid (0P) and perforated (3CP) PHSs models

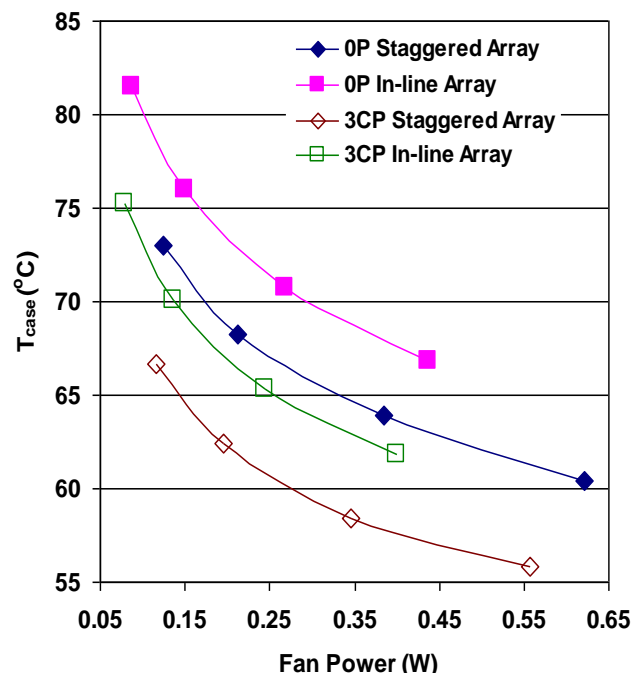


Fig. 14: Effect pins array on  $T_{case}$  and  $P_{fan}$  for solid (0P) and perforated (3CP) PHSs models

These figures demonstrate that the perforated fins investigated here can provide substantial improvements in heat transfer with significant reductions in power consumption and heat sink mass.

#### IV. CONCLUSIONS

Pinned Heat Sinks (PHSs) provide the cooling required in many critical applications. The present study demonstrates that perforating the pin fins in a PHS can provide substantial improvements in heat transfer, power consumption and weight, at the price of increased manufacturing complexity. It has been shown that the shape of the perforations can also have an important influence on heat sink performance. Circular perforations provide the greatest enhancement in heat transfer, since they maximize the speed of the air jets flowing through the perforations, while the elliptical perforations considered provide the greatest reduction in pressure drop since they offer the least resistance to air flowing through them.

Further performance enhancements can be achieved by staggering the pins, which enhances turbulent mixing around the pins at the price of a larger pressure drop. However, results have shown that the enhancement in heat transfer is dominant in the sense that this approach enables the heat sink base temperature to be cooled to a target temperature for a significantly lower power consumption.

Table 2: Enhancement of  $Nu_T$ ,  $P_{fan}$ , and  $T_{case}$  for perforated pin

| Heat Sinks Designs             | Parameter Studies |                 |                          |                                       |
|--------------------------------|-------------------|-----------------|--------------------------|---------------------------------------|
|                                | $\uparrow A_T$    | $\uparrow Nu_T$ | $\downarrow P_{fan}$ (W) | $\downarrow T_{case}$ ( $^{\circ}C$ ) |
| Circular Perforated Pins (3CP) | 15%               | 9%              | 9%                       | 8%                                    |
| Square Perforated Pins (3SP)   | 18%               | 4%              | 7%                       | 5%                                    |
| Elliptic Perforated Pins (3EP) | 17%               | 4%              | 12%                      | 5%                                    |

Table 3: The reduction of  $T_{case}$  and the increase in  $P_{fan}$  of the staggered array of pins compared with the in-line array for 0P and 3CP PHSs

| Heat Sinks Designs                      | Parameter Studies      |                                       |
|-----------------------------------------|------------------------|---------------------------------------|
|                                         | $\uparrow P_{fan}$ (W) | $\downarrow T_{case}$ ( $^{\circ}C$ ) |
| Staggered array of solid Pins (0P)      | 30%                    | 10%                                   |
| Staggered array of perforated Pins (3P) | 30%                    | 12%                                   |

#### ACKNOWLEDGEMENTS

The authors would like to thank the Higher Committee for Education Development in Iraq (HCED), Iraqi Ministry of Higher Education and Scientific Research (MOHE), and Mechanical Engineering Department University of Anbar, Iraq for financial support of this work.

#### REFERENCES

- [1] Shaeri, M.R. and M. Yaghoubi, Thermal enhancement from heat sinks by using perforated fins. *Energy Conversion and Management*, 2009. 50(5): p. 1264-1270.
- [2] Shaeri, M.R. and M. Yaghoubi, Numerical analysis of turbulent convection heat transfer from an array of perforated fins. *International Journal of Heat and Fluid Flow*, 2009. 30(2): p. 218-228.
- [3] Amer Al-damook, Kapur N., Summers J.L., Thompson H.M., An experimental and computational investigation of thermal airflows through perforated pin heat sinks, in *progressing of Applied Thermal Engineering Journal*, 89 (2015) 365–376.
- [4] Amer Al-damook, Kapur N., Summers J.L., Thompson H.M., Computational design and optimisation of pin fin heat sinks with rectangular perforations, *Applied Thermal Engineering Journal*, (2016).
- [5] Shaeri, M.R. and M. Yaghoubi, Thermal enhancement from heat sinks by using perforated fins. *Energy Conversion and Management*, 2009. 50(5): p. 1264-1270.
- [6] Shaeri, M.R. and M. Yaghoubi, Numerical analysis of turbulent convection heat transfer from an array of perforated fins. *International Journal of Heat and Fluid Flow*, 2009. 30(2): p. 218-228.
- [7] Shaeri, M.R. and T.C. Jen, The effects of perforation sizes on laminar heat transfer characteristics of an array of perforated fins. *Energy Conversion and Management*, 2012. 64: p. 328-334.
- [8] Shaeri, M.R. and T.C. Jen, Turbulent Heat Transfer Analysis of a Three-Dimensional Array of Perforated Fins Due to Changes in Perforation Sizes. *Numerical Heat Transfer, Part A: Applications*, 2012. 61(11): p. 16.
- [9] Ismail, F., M.O. Reza, M.A. Zobaer, and Mohammad Ali, Numerical investigation of turbulent heat convection from solid and longitudinally perforated rectangular fins. *IEEE 5th BSME International Conference on Thermal Engineering*, 2013. p.497-502.
- [10] Ismail, F., Effects of Perforations on the Thermal and Fluid Dynamic Performance of a Heat Exchanger. *IEEE Transaction on Component, Packaging and Manufacturing Technology*, 2013. p.1-8
- [11] Ismail, M. F., Hasan M. N., & Ali M., Numerical simulation of turbulent heat transfer from perforated plate-fin heat sinks. *Heat and Mass Transfer*, 2014. 50(4), p. 509-519.
- [12] Yaghoubi M., Shaeri M. R., & Jafarpur K., Three-dimensional numerical laminar convection heat transfer around lateral perforated fins. *Computational Thermal Sciences: An International Journal*, 2009. 1(3): p323-340
- [13] Yaghoubi M., Shaeri M. R., & Jafarpur K., Heat transfer analysis of lateral perforated fin heat sinks. *Applied Energy*, 2009. 86(10): p. 2019-2029.

[14] Ismail, M. F., Hasan M. N., & Saha S. C., Numerical study of turbulent fluid flow and heat transfer in lateral perforated extended surfaces. *Energy*, 2014. 64: p. 632-639.

[15] Sahin, B. and A. Demir, Thermal performance analysis and optimum design parameters of heat exchanger having perforated pin fins. *Energy Conversion and Management*, 2008a. 49(6): p. 1684-1695.

[16] Sahin, B. and A. Demir, Performance analysis of a heat exchanger having perforated square fins. *Applied Thermal Engineering*, 2008b. 28(5-6): p. 621-632.

[17] Amol B. Dhumme and Hemant S. Farkade, Heat Transfer Analysis of Cylindrical Perforated Fins in Staggered Arrangement. *International Journal of Innovative Technology and Exploring Engineering (IJITEE)*, 2013. 2(5): p. 225-230.

[18] Waleed Al-Sallami, Amer Al-damook, Thompson H.M., A Numerical Investigation of Thermal Airflows over Strip Fin Heat Sinks, *International Communications in Heat and Mass Transfer*, (2016).

[19] Zhou, F. and I. Catton, Numerical Evaluation of Flow and Heat Transfer in Plate-Pin Fin Heat Sinks with Various Pin Cross-Sections. *Numerical Heat Transfer, Part A: Applications*, 2011. 60(2): p. 107-128.

[20] Leung, C. W., & Probert, S. D., Heat-exchanger performance: effect of orientation. *Applied energy*, 1989. 33(4), 235-252.

[21] Menter, F. R., Zonal Two Equation k- $\omega$  Turbulence Models for Aerodynamic Flows, *AIAA* 1993, p.93-2906.

[22] ANSYS FLUENT User's Guide, 2011.

[23] Holman, J. P., *Experimental Methods for Engineers*, McGraw Hill Book Company, 10971, 8th edition, 2011.

[24] Sparrow, E. M., Ramsey, J. W., & Altemani, C. A. C., Experiments on in-line pin fin arrays and performance comparisons with staggered arrays, *Journal of heat transfer*, 1980. 102(1): p.44-50.

[25] Yang, Y. T., & Peng, H. S., Investigation of planted pin fins for heat transfer enhancement in plate fin heat sink. *Microelectronics Reliability*, 2009. 49(2): p. 163-169.

[26] Yang, K.S., Chu, W.H., Chen, Y. and Wang, C.C.. A comparative study of the airside performance of heat sinks having pin fin configurations. *International Journal of Heat and Mass Transfer*, 2007. 50(23), pp.4661-4667.

[27] Sara, O. N., Pekdemir, T., Yapici, S. and Ersahan, H., Thermal Performance Analysis for Solid and Perforated Blocks Attached on a Flat Surface in Duct Flow. *Energy Conversion & Management*, 2012. 41(10): p. 1010-1028.

## V. NOMENCLATURE

|                          |                                                                  |
|--------------------------|------------------------------------------------------------------|
| $A_p$                    | cross-sectional area of the flow passage of the heat sink, $m^2$ |
| $D$                      | pin diameter of the pin fin heat sink, mm                        |
| $D$                      | perforation diameter of the pin fin, mm                          |
| $D_h$                    | hydraulic diameter, m                                            |
| $F$                      | friction factor                                                  |
| $H$                      | pin fin height, mm                                               |
| $H$                      | heat transfer coefficient, $W/m^2.K$                             |
| $K$                      | turbulence kinetic energy                                        |
| $N$                      | number of perforations                                           |
| $N$                      | number of pins                                                   |
| $L$                      | heat sink length, mm                                             |
| $Nu$                     | Nusselt number                                                   |
| $P_{fan}$                | fan power, W                                                     |
| $\Delta P$               | pressure drop, Pa                                                |
| $Pr$                     | Prandtl number                                                   |
| $Pr_t$                   | turbulent Prandtl number                                         |
| $Q$                      | power applied on the base, W                                     |
| $S_y$                    | pin pitch in streamwise direction, mm                            |
| $S$                      | an invariant measure of the strain rate                          |
| $Re$                     | Reynolds number                                                  |
| $T$                      | temperature, $^{\circ}C$                                         |
| $\Delta T$               | temperature difference, K                                        |
| $U$                      | air velocity inlet, m/s                                          |
| $\alpha$                 | fluid thermal diffusivity ( $m^2/s$ )                            |
| $\alpha, \beta, \beta^*$ | turbulence model constant                                        |
| $\phi$                   | porosity $V_{void}=V$                                            |
| $\mu$                    | fluid viscosity (Pa.s)                                           |
| $\mu_t$                  | turbulent eddy viscosity, Pa/s                                   |
| $\rho$                   | fluid density ( $kg/m^3$ )                                       |
| $N$                      | kinematic viscosity, $m^2/s$                                     |
| $\nu_t$                  | turbulent kinematic viscosity, $m^2/s$                           |
| $\epsilon_{\sigma}$      | k- $\epsilon$ turbulence model constant                          |
| $k_{\sigma}$             | turbulence model constant for the k-equation                     |
| $\omega_{\sigma}$        | k- $\omega$ turbulence model constant                            |